中國機械工程學刊第四十卷第六期第 683~692 頁(民國一百零八年)
Journal of the Chinese Society of Mechanical Engineers, Vol.40, No.6, pp 683~692 (2019)

Study on Navigation Line Detection in L.barbarum Garden Based on Genetic Algorithm

Mao-Qiang Li*and Zhi-Feng Liu**

Keywords：Lycium barbarum garden, Self-moving platform, image segmentation, navigation line detection.

ABSTRACT

The form for a "general self-moving host platform + operation module" must be established to realize intelligent production in the Lycium barbarum (*L.barbarum*). Region segmentation between the plant column and the soil and detection of the navigation line are two challenges to realizing the autonomous navigation of self-moving platforms. For region segmentation between the plant column and the soil, a segmentation method that based on neural networks and Otsu's method is proposed. Experiments are performed that demonstrate effective image segmentation using this approach. A noise removal technique is proposed that can effectively remove the noise from the plant column region and the noise from the soil region. A parameterized octagonal template is constructed for the navigation line detection problem after image segmentation, which is matched to the segmentation image. The matching overlap is defined as the fitness function, and the octagonal template parameter is optimized based on a genetic algorithm. Then, the octagon midline is extracted from the optimized octagonal template as the navigation line. The experiments demonstrate that the method can effectively detect the navigation line using this method, which lays a foundation for the precise navigation of self-moving platforms in complex and unstructured *L.barbarum* Garden environments.

INTRODUCTION

L.barbarum is a treasure of traditional Chinese medicine. The fruit contains carotene, ascorbic acid, and other nutrients that possess remarkable health care functions. The planting area and production of Ningxia is the largest *L.barbarum* region in China and accounts for more than 50% of its total production. *L.barbarum* is the most traditional, advantageous industry in Ningxia, which is the key industry it supports. Driven by projects of "High-quality brand *L.barbarum* base construction" and "*L.barbarum* southward movement project", the *L.barbarum* industry has developed rapidly. For example, the planting area has increased tenfold over the past 10 years and has reached 333 km². In addition, the total output has increased by an average annual growth rate of 25.7% to 80 million kg per year. Currently, *L.barbarum* and its products have been exported to 23 countries and regions, such as the United States, Canada and Australia, with broad market prospects.

At present, the traditional inefficient operational modes in the processes of *L.barbarum* plant protection, fertilization, picking and other production links have become the bottle-neck that restricts further industrial development. Developing intelligent production equipment in the form of a "general self-moving host platform + operation module" is an urgent task for healthy improvements to the *L.barbarum* industry. To adapt to complex unstructured environments, self-moving platforms should have the capability of autonomous navigation. Solving the problem of navigation line detection under the *L.barbarum* environment is the key to autonomous navigation.

According to (Ebrahimpou et al., 2012; Ding et al., 2016; Gou & Cheng, 2018; Liu et al., 2018; Miao et al., 2018), navigation in outdoor environments is a challenging task for an autonomous mobile robot because of the highly unstructured and different characteristics of outdoor environments. And vision is the most important information source for navigation in unstructured environments (Roviramás et al., 2004; Yohannan & Chandy, 2017; Yang et al., 2018; Mannar et al., 2018). Researchers carried out path recognition and planning for farmland robots based on computer vision (Zhai et al., 2016; Tang & Ji, 2018; Zhao et al., 2016; Erhan et al., 2017; Zhou et al., 2014; Jiang et al., 2016; Ball et al., 2016; Zhang et al., 2018). (Li et al., 2012) present an image detection algorithm for navigation route of cotton

Paper Received May, 2019. Revised September, 2019, Accepted September, 2019, Author for Correspondence: Zhi-Feng Liu.

* *Graduate student, School of Mechanical Engineering, Hefei University of Technology, Hefei, Anhui 230009, China.*

** *Professor, School of Mechanical Engineering, Hefei University of Technology, Hefei, Anhui 230009, China.*

harvester, which extracted target features of different fields by the color difference 3B-R-G and obtained navigation line by using passing a Known Point Hough Transform. (Winterhalter et al., 2018) present a novel algorithm for robust crop row detection that adapts the Hough transform for line detection to detect a pattern of parallel equidistant lines which is able to jointly estimate the angle, lateral offset and crop row spacing for tiny plants. (Yang et al., 2018) used the red feature to extract the roots of the maize plants, and used the least square method to fit these positioning points to extract the root row lines, then get the actual navigation centerline by calculating the slopes of the root row lines. (Meng et al., 2018) proposed a method of crop lines identification based on improved genetic algorithm which randomly selected two points from image bottom and top side to code as a chromosome. According to the above methods and algorithms for agricultural robot vision navigation have been applied to corn, wheat, cotton and other crops which are under row sown environments. Image sensor is mounted higher than plants which are low crops or at primary stage of growth. Therefore, there are several rows, ridges or furrows in the image collected. And the rows, ridges or furrows are evident, providing a better recognition basis for visual detection. Under the above crop environment and collection conditions, these researchers made the most of the better recognition to carry out navigation line detection based on Hough Transform and the least square method which are all based on fitting lines, with ideal detection effect.

However, the plants of *L.barbarum* are shrubs with shape, size, plant location, and especially height distinct from the above crops. The planting of *L.barbarum* does not strictly follow the linear features. The growth of branch is disorderly. The *L.barbarum* plants are taller than the crops described above. If image sensor is mounted higher than *L.barbarum* plants, shoot the plant columns from the top of the plant. The collected image has several plant columns without strict linear features. And the motion blur caused by the height of the image sensor and the sloshing of the machine is very serious. These factors are not conducive to subsequent image processing and navigation line detection. Therefore, the mounting height of the image sensor can only be lower than that of the *L.barbarum* plant. For reasons of planting, growth, and image sensor mounting height, there are only plant columns on both sides and the soil in the middle in the image collected from the environment of *L.barbarum* Garden, with no obvious linear features.

Navigation line detection methods proposed by these researchers, such as Hough Transform, the least square method and so on based on fitting one line are specific to crops with evident rows, ridges or furrows which provide better recognitions basis for visual detection. It cannot adapt to the environment of *L.barbarum* Garden. Therefore, these Navigation line detection methods cannot be directly transplanted to images collected *L.barbarum* Garden. In addition, in the growth cycle, the leaf color of *L.barbarum* plant column has green, light green and yellow-green. Also soil color varies slightly from location to location. Single color difference models used by these researchers, such as 3G-B-R model, have limited generalization ability for segmentation between the plant column and the soil.

Therefore, though the above image processing methods and navigation line detection methods proposed by these previous researchers provide important reference information, it cannot be directly transplanted to images collected from *L.barbarum* Garden. And the navigation problems presented by the complex and unstructured *L.barbarum* Garden environments have not been previously studied. This paper is focused on the problem of navigation line detection for self-moving platforms in complex and unstructured *L.barbarum* Garden environments. We perform a study on the contents of image segmentation between the plant column and the soil, on noise removal, and on navigation line detection.

IMAGE ACQUISITION

L.barbarum Garden images were collected on May to June, 2018, from a site located in the Bairuiyuan *L.barbarum* Garden in the Xixia district, Yinchuan, Ningxia using a Redmi 3X camera. The images were captured in JPG format with 208×416 pixels. Fig. 1 shows an original image collected from the *L.barbarum* Garden in a natural setting. The green regions on both sides are for the plant column, which contains a small amount of bare surface. The middle grey-yellow region is the soil, which contains a few dispersed weeds. There is a strong color contrast ratio between the plant column region and the soil region. The edge between the plant column region and the soil region is an important feature that reflects the navigation position and direction.

Fig. 1. Image from a *L.barbarum* Garden.

SEGMENTATION BETWEEN THE PLANT COLUMN REGION AND THE SOIL REGION

Segmentation Method

The processing flowchart for the segmentation problem between the plant column region and the soil region is shown in Fig. 2.

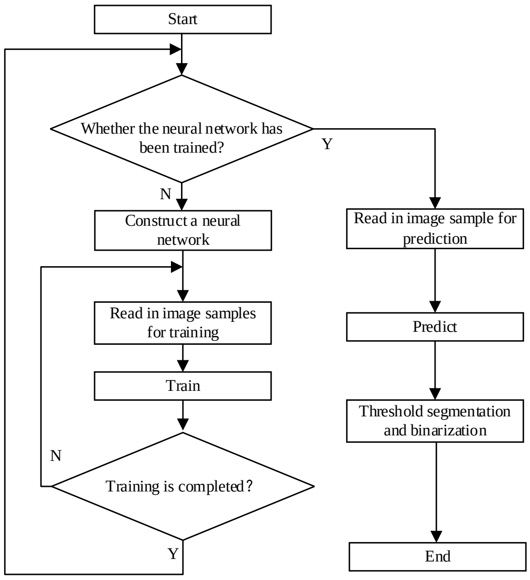

Fig. 2. Processing flowchart for image segmentation.

Image Segmentation Based on Back Propagation Neural Network(BP) and Otsu's Method

Four categories of images are selected as samples. The first category is 30 images acquired at the morning or evening, are selected. The second category is 30 images with more light intensity but less shadow. The third category is 30 images with high light intensity and more shadows. The fourth category is 30 images under cloudy conditions. In each category, 25 images are selected, and a total of 100 images are selected in the four cases. The 100 images are put in random order No.1, No.2, No.3... No.100 as the training set. The remaining 5 images in each category are selected, and a total of 20 images in the four categories. The 20 images are put in random order No.101, No.102, No.103 ... No.120 as the test set.

The edges in all 120 images were calibrated manually to perform image segmentation. The manual edge calibration effect of image No.1 is shown in Fig. 3(a), and its manual image segmentation effect is shown in Fig. 3(b).

(a)

(b)

Fig. 3. Manual edge calibration and image segmentation effect for image No.1.

(a) Manual edge calibration and (b) manual image segmentation effect for image No.1

$$\left\{ \begin{matrix} R(i-1,j-1) \\ G(i-1,j-1) \\ B(i-1,j-1) \\ R(i-1,j) \\ G(i-1,j) \\ B(i-1,j) \\ R(i-1,j+1) \\ G(i-1,j+1) \\ B(i-1,j+1) \\ R(i,j-1) \\ G(i,j-1) \\ B(i,j-1) \\ R(i,j) \\ G(i,j) \\ B(i,j) \\ R(i,j+1) \\ G(i,j+1) \\ B(i,j+1) \\ R(i+1,j-1) \\ G(i+1,j-1) \\ B(i+1,j-1) \\ R(i+1,j) \\ G(i+1,j) \\ B(i+1,j) \\ R(i+1,j+1) \\ G(i+1,j+1) \\ B(i+1,j+1) \end{matrix} \right\}. \tag{1}$$

A three-layer BP neural network is constructed for automatic edge detection and image segmentation. The input layer has 27 neurons. The red (R), green (G) and blue (B) component values of a 3x3 neighborhood of pixel (i,j) are selected as the input, as shown in Eq. (1). The Back propagation neural network hidden layer also has 27 neurons, and the output is a grayscale result of pixel (i,j), which ranges from 0 to 1. The closer the output value is to 0, the more likely the pixel is to be part of the soil region. Conversely, the closer the output value is to 1, the more likely it is to be part of the plant column region. The double bending function was selected as the neuron input and output function, as shown in Eq. (2). The square error sum of the output layer neuron result and teacher signal are defined as shown in Eq. (3).

$$f(x) = \frac{1}{1+e^{-x}}. \tag{2}$$

$$E=\frac{1}{2}(d-o)^2, \tag{3}$$

where o is the output layer neuron result and d is the given output layer teacher signal.

Images No.1 to No.100 is selected and their manual image segmentation results are treated as the training set. As shown in Fig. 4(a), after 100 iterations, the error drops to 0.157, which provides convergent and effective network weights. Fig.4(b) shows the error variation curve, indicating that the error decreases rapidly in the first 10 training iterations. After these iterations, the error curve becomes relatively flat. Therefore, it can be seen that the number of trainings should be limited to save on computational costs.

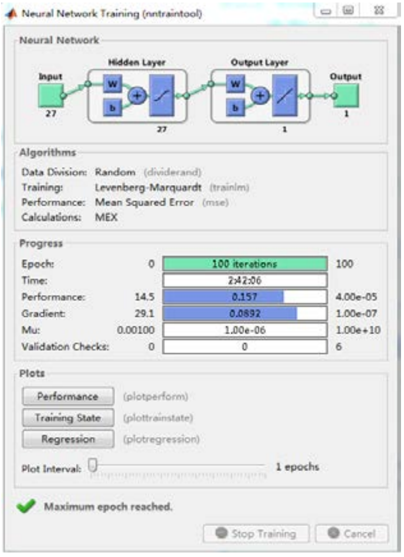

(a)

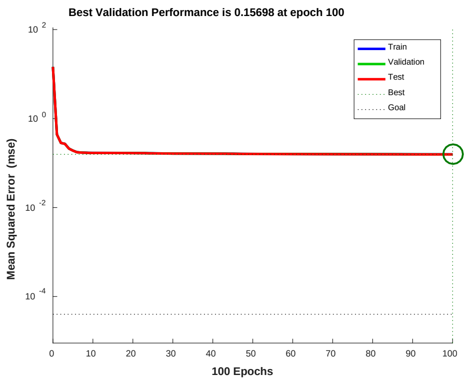

(b)

Fig. 4. Neural network training results.
(a) Operation results diagram of the network training and (b) the error variation curve

The network is used after training to predict image segmentation for images No.101 to No.120. The prediction results of image No.101 are shown in Fig. 5, and the image segmentation results using Otsu's method are shown in Fig. 6.

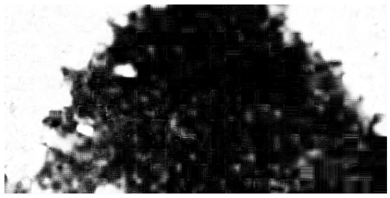

Fig. 5. Prediction result of image No.101 using the proposed method.

Fig. 6. Segmentation result of image No.101 using Otsu's method.

To evaluate the segmentation precision using the above neural network and Otsu's method, the test precision evaluation coefficient was computed using Eq. (4). The closer the coefficient is to 1, the closer image segmentation result is to that of the manual segmentation result.

$$f_{precision}=1-\frac{sum(sum(figure_{manual}\,xor\,figure_{BP/Otsu}))}{86528}, \tag{4}$$

where $figure_{manual}$ is the manual segmentation result, $figure_{BP/Otsu}$ is the image segmentation result based on the neural network and Otsu's method, $sum(sum(x))$ is a function that sums all elements of the matrix x, and the value 86,528 is the number of pixels in a 208×416 image.

Using the above method, the precision evaluation coefficient is calculated for image No.101 to No.120. The statistical results from performing this process on 20 images are presented in Table 1. As can be seen, the average of the precision evaluation coefficients is 95.05%. The segmentation method based on the neural network and Otsu's method has a high precision and meets the requirements of post-processing.

Table 1. Segmentation precision evaluation coefficients statistics

Image sequence number	Precision evaluation coefficients	Image sequence number	Precision evaluation coefficients
101	94.56%	111	95.07%
102	96.18%	112	96.17%
103	96.61%	113	95.59%
104	96.20%	114	93.87%
105	91.71%	115	96.39%
106	92.52%	116	94.19%
107	97.31%	117	92.73%
108	94.98%	118	97.58%
109	95.45%	119	93.81%
110	94.74%	120	95.41%
Average		95.05%	

NOISE REMOVAL

It can be seen from Fig. 6 that the white area on both sides of the image with pixel values of “1” are primarily the plant column region, and the black area in the middle of the image with pixel values of “0” are primarily the soil region. A few white areas are embedded in the soil regions, which are mainly from weeds. Additionally, a few black areas are embedded in the plant regions, which are mainly from the bare surfaces. The above few white and black areas are considered to be noise. This noise is not conducive to the subsequent edge extraction and requires further processing. The processing flowchart is shown in Fig. 7.

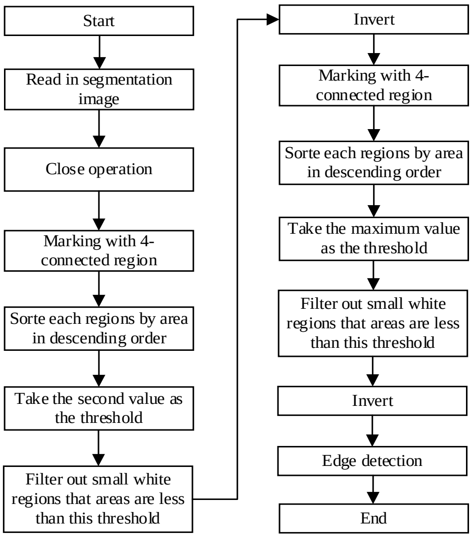

Fig. 7. Processing flowchart for noise removal.

The results of a closing operation using a flat disk structure element with a radius of 8 pixels for the image shown in Fig. 6 are shown in Fig. 8. The image in Fig. 8 is marked with a 4-connected region, and shown in Fig. 9. Every connected region shown in Fig. 9 is counted and sorted in descending order, as shown in Table 2. Since the area of the plant column regions on both sides is much larger than area of the noise in the soil region, the first and second values represent the plant column area on both sides of the soil, and the remaining values are the areas of the noise in the soil region. Thus, the second value is taken as the threshold and the noise areas less than the threshold are filtered out, as shown in Fig. 10. The image is then inverted, which is shown in Fig. 11. The image in Fig. 11 is marked with a 4-connected region and shown in Fig. 12. Every connected region is counted and sorted in descending order, as shown in Table 3. The maximum value is the area of the soil region, while the second, third, and fourth values are the areas of the noise in the plant column region. The maximum value is taken as the threshold and the noise regions less than the threshold are filtered out, as shown in Fig. 13. The image is then inverted, as shown in Fig. 14. Edge detection is next performed on the image, and the results are shown in Fig. 15. The manual image segmentation results for image No. 101 are shown in Fig. 16, and a comparison of the manual edge (red line) and the automated edge detection results using the proposed method (blue) are shown in Fig. 17. Image segmentation and edge detection is performed using the method described above for image No.102 to No.120. The edge detection effects for a few select images are shown in Figs. 18 to 21.

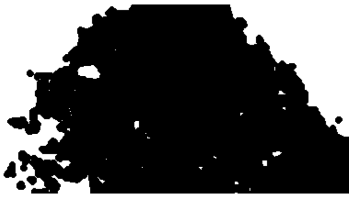

Fig. 8. Closing operation results.

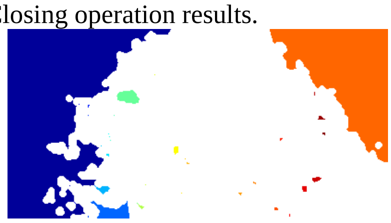

Fig. 9. 4-connected region marking results.

Table 2. Area information statistics of the connected regions

Regions number	Area	Regions number	Area
1	18403	21	3
2	9921	22	2
3	481	23	1
4	262	24	1
5	74	25	1
6	37	26	1
7	37	27	1
8	28	28	1
9	20	29	1
10	14	30	1
11	11	31	1
12	7	32	1
13	7	33	1
14	7	34	1
15	6	35	1
16	5	36	1
17	4	37	1
18	4	38	1
19	4	39	1
20	3	40	1

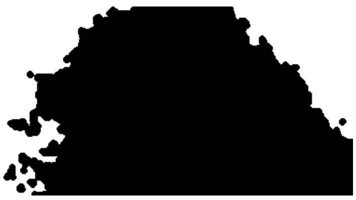

Fig. 10. Results of the noise removal for the soil region.

Fig. 11. The inverted image.

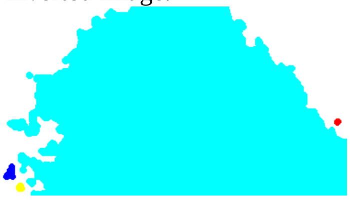

Fig. 12. Results of the 4-connected region marking for the inverted image.

Table 3. Area information statistics of the connected regions for the inverted image

Regions number	Area
1	56661
2	170
3	80
4	49

Fig. 13. Results of noise removal for the plant column region.

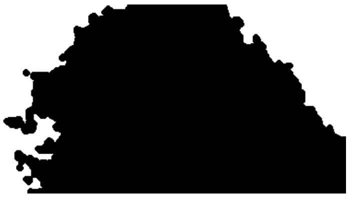

Fig. 14. Results of noise removal.

Fig. 15. Edge detection results.

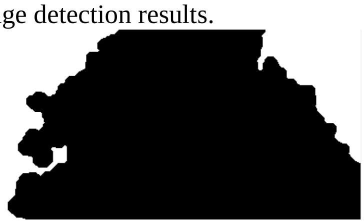

Fig. 16. The manual image segmentation results for image No.101.

Fig. 17. The comparison of edge detection results for image No.101.

Fig. 18. The comparison of edge detection results for image No.105.

Fig. 19. The comparison of edge detection results for image No.110.

Fig. 20. The comparison of edge detection results for image No.115.

Fig. 21. The comparison of edge detection results for image No.120.

To evaluate the effectiveness of the segmentation for image No.101 using the method described in this paper, the manual image segmentation result shown in Fig. 16 is set as the real value and the test quality evaluation coefficient is computed as:

$$f_{quality} = 1 - \frac{sum(sum(figure_{manual}\,xor\,figure_{noise-removed}))}{86528}, \quad (5)$$

where $figure_{manual}$ is the manual segmentation results, $figure_{noise-removed}$ is the image after noise removal, $sum(sum(x))$ is a function that sums all elements of the matrix x, and the value 86,528 is the number of pixels in a 208×416 image.

The quality evaluation coefficients are calculated for image No.102 to No.120 and are presented in Table 4. It can be seen that the minimum value of the quality evaluation coefficients is 92.94% and the average value is 97.09% after noise removal, indicating a high fitting degree to the results of the manual segmentation. Thus, the method described above has a strong adaptability to image segmentation, noise removal, and edge detection.

Table 4. Quality evaluation coefficient statistics

Image sequence number	Quality evaluation coefficients	Image sequence number	Quality evaluation coefficients
101	94.31%	111	98.62%
102	96.55%	112	97.02%
103	98.11%	113	97.06%
104	97.75%	114	98.57%
105	95.87%	115	98.14%
106	92.94%	116	97.47%
107	98.33%	117	96.52%
108	97.51%	118	97.58%
109	96.15%	119	97.80%
110	97.08%	120	98.36%
Average		97.09%	

NAVIGATION LINE DETECTION

Navigation Line Detection Method

For the navigation line detection problem after image after segmentation, a parameterized octagonal template is constructed and matched with the segmentation image. The matching overlap is defined as the fitness function, and the octagonal template parameter is optimized using a genetic algorithm. Then, the octagon midline is extracted from the optimized octagonal template as the navigation line. The processing flowchart is shown in Fig. 22.

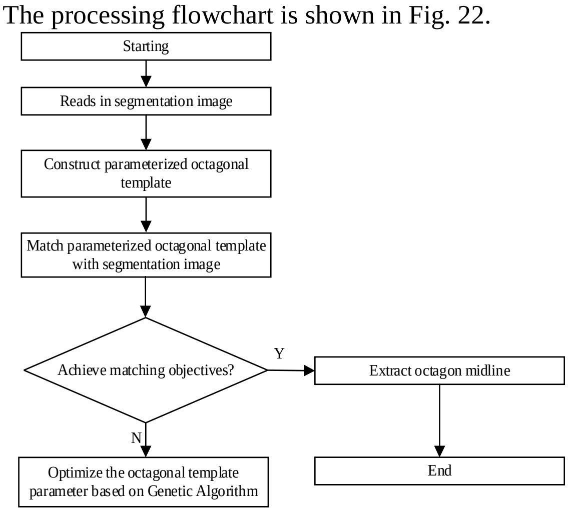

Fig. 22. Navigation line detection method.

Parameterized Octagonal Template Construction

As shown in Fig. 13, the white area is the soil region and the black area is the plant column region. The parameterized octagonal template is matched with the image in Fig. 13, and is shown in Fig. 23. The greater the overlapping area is for the octagonal *ABCDEFGH* with the soil region, the more matching overlap there is with the octagonal and the soil region. The midline *IJKL* of the octagonal with the highest match can be used as the navigation line. Thus, the most optimal octagonal template is the key to the navigation line detection. The coordinate system is established where the eight vertices of the octagon are $A=(x_1,0)$, $B=(x_2,0)$, $C=(x_3,69)$, $D=(x_4,138)$, $E=(x_5,207)$, $F=(x_6,207)$, $G=(x_7,138)$, and $H=(x_8,69)$.

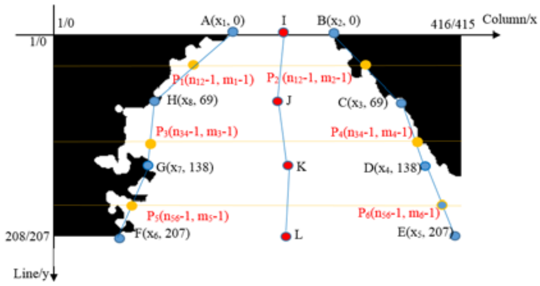

Fig. 23. Template matching for the segmented image.

The intersection point coordinate of line AB with each line is $P_1(n_{12}-1, m_1-1)$, and the intersection point coordinate of line BC with each line is $P_2(n_{12}-1, m_2-1)$. Thus, the $ABCH$ part of the parameterized octagonal template is as follows:

$$figure_{tem}(n_{12}, m) = \begin{cases} 0 & 1 < m < m_1 \\ 1 & m_1 < m < m_2 \\ 0 & m_2 < m < 416 \end{cases}, \quad (6)$$

$$m_1 = round((((n_{12}-1)(x_8-x_1))/69)+x_1)+1, \quad (7)$$

$$m_2 = round((((n_{12}-1)(x_3-x_2))/69)+x_2)+1, \quad (8)$$

where n_{12} is the line coordinate of P_1 and P_2 in the parameterized octagonal template with $n_{12}=1,2...70$, m is the column coordinate of the parameterized octagonal template with $m=1,2...416$, and m_1 and m_2 are the column coordinates of P_1 and P_2, respectively.

The intersection point coordinate of line HG with each line is $P_3(n_{34}-1, m_3-1)$, and the intersection point coordinate of line CD with each line is $P_4(n_{34}-1, m_4-1)$. Thus, the $HCDG$ part of the parameterized octagonal template is as follows:

$$figure_{tem}(n_{34}, m) = \begin{cases} 0 & 1 < m < m_3 \\ 1 & m_3 < m < m_4 \\ 0 & m_4 < m < 416 \end{cases}, \quad (9)$$

$$m_3 = round((((n_{34}-1-69)(x_7-x_8))/69)+x_8)+1, \quad (10)$$

$$m_4 = round((((n_{34}-1-69)(x_4-x_3))/69)+x_3)+1, \quad (11)$$

where n_{34} is the line coordinate of P_3 and P_4 in the parameterized octagonal template with $n_{34} = 70, 71...139$, m is the column coordinate of the parameterized octagonal template with $m = 1, 2...416$, and m_3 and m_4 are the column coordinates of P_3 and P_4, respectively.

The intersection point coordinate of line GF with each line is $P_5(n_{56}-1, m_5-1)$, and the intersection point coordinate of line DE with each line is $P_6(n_{56}-1, m_6-1)$. Thus, the $HCDG$ part of the parameterized octagonal template is as follows:

$$figure_{tem}(n_{56}, m) = \begin{cases} 0 & 1 < m < m_5 \\ 1 & m_5 < m < m_6 \\ 0 & m_6 < m < 416 \end{cases}, \quad (12)$$

$$m_5 = round((((n_{56}-1-138)(x_6-x_7))/69)+x_7)+1, \quad (13)$$

$$m_6 = round((((n_{56}-1-138)(x_5-x_4))/69)+x_4)+1, \quad (14)$$

where n_{56} is the line coordinate of P_5 and P_6 in the parameterized octagonal template with $n_{56} = 139, 140...208$, m is the column coordinate of the parameterized octagonal template with $m = 1, 2...416$, and m_5 and m_6 are the column coordinates of P_5 and P_6, respectively.

It can be seen from Eq. (6), (7), (8), (9), (10), (11), (12), (13), and (14) that finding the optimal parameters of x_1, x_2, x_3, x_4, x_5, x_6, x_7, and x_8 is the key to navigation line detection.

Parameter Optimization Based on Genetic Algorithm

To determine the appropriate x_1, x_2, x_3, x_4, x_5, x_6, x_7, and x_8, multiple evolutionary searches are performed based on the genetic algorithm. The fitness function is defined as follows:

$$Fit(x) = \frac{(figure_{tem} \ \& \ figure_{noise-removed})}{(figure_{tem} \mid figure_{noise-removed})}. \quad (15)$$

The roulette selection and single point cross methods are used. The crossover probability is set to 0.7, and the basic bit variation method is adopted. The mutation probability is set to 0.01 and the population size of 50 and end algebra of 250 are chosen. The range the of parameter variables is given as:

$$x = \begin{bmatrix} 0.1,415;0.1,415;0.1,415;0.1,415;0.1,415; \\ 0.1,415;0.1,415;0.1,415 \end{bmatrix}. \quad (16)$$

An optimization experiment is performed for the segmentation image shown in Fig. 13 to determine the octagonal template parameters. The fitness curve progression during the iterative operations is shown in Fig. 24. The optimization results are shown in Eq. (17), and the optimized parameterized octagonal template is shown in Fig. 25.

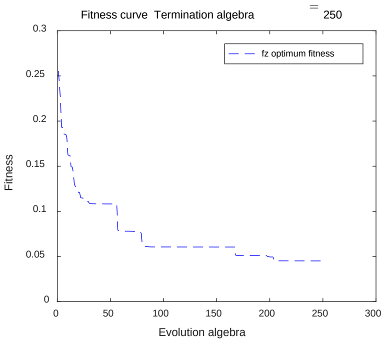

Fig. 24. Fitness curve progression.

$$\begin{cases} x_1 = 148 \\ x_2 = 278 \\ x_3 = 367 \\ x_4 = 407 \\ x_5 = 407 \\ x_6 = 70 \\ x_7 = 41 \\ x_8 = 87 \end{cases}. \quad (17)$$

Fig. 25. The optimized parameterized octagonal template.

Based on the above method, an optimization experiment is performed to determine the octagonal template parameters for image No.102 to No.120, and the results are shown in Table 5. The minimum percentage of the parameterized octagonal template matching with the segmentation image was 84.71% with an average of 92.33%, indicating a high degree of matching. Thus, the results meet the requirements for navigation line detection. Based on the optimization parameters shown in Table 5, the octagonal template is used to detect the navigation line for each of the 20 images. The detection effect for image No.105, No.110, No.115, and No.120 are shown in Figs. 26 to 29. As can be seen, the proposed method can stably and reliably detect the navigation lines for the *L.barbarum* Garden using the optimized parameterized octagonal template.

Table 5. Results of the parameter optimization

Image sequence number	x_1	x_2	x_3	x_4	x_5	x_6	x_7	x_8	Percentage of matching
101	148	278	368	407	407	70	42	87	93.81%
102	161	295	348	389	414	20	84	33	88.66%
103	202	226	316	353	342	19	78	91	92.96%
104	130	248	333	399	408	15	45	55	87.21%
105	195	263	321	379	363	94	76	146	94.27%
106	149	248	314	389	384	116	26	72	87.97%

107	175	287	311	408	401	132	85	126	91.63%
108	189	267	336	332	394	118	68	92	93.66%
109	202	355	331	355	358	98	43	182	93.19%
110	220	275	308	324	362	48	90	193	95.35%
111	151	296	363	411	392	103	38	88	93.86%
112	167	249	292	374	378	76	5	131	91.66%
113	153	216	325	350	351	9	59	94	95.42%
114	118	291	268	400	406	18	101	66	84.71%
115	217	261	328	366	343	180	99	131	94.61%
116	196	257	304	330	376	131	75	147	92.99%
117	162	251	340	392	403	156	151	172	93.03%
118	184	236	307	341	395	41	76	105	95.80%
119	139	313	245	376	394	25	41	135	89.82%
120	205	247	328	396	404	112	145	163	96.03%
	Average								92.33%

Fig. 26. Navigation line detection effect fir image No. 102 (The second type).

Fig. 27. Navigation line detection effect for image No. 105(The first type).

Fig. 28. Navigation line detection effect for image No. 110(The fourth type).

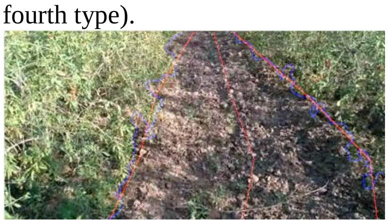

Fig. 29. Navigation line detection effect for image No. 120(The third type).

CONCLUSIONS

(1) A segmentation method based on a neural network and Otsu's method is proposed for the image segmentation problem between the plant column region and the soil region in *L.barbarum* Garden environments.

(2) Experiments show that the proposed method can effectively realize image segmentation with the average of segmentation precision evaluation coefficient reaching 95.05%.

(3) A noise removal method for the plant column region and the soil region is proposed. The method can effectively remove noise in the plant column region and noise in the soil region with an average quality evaluation coefficient reaching 97.09%.

(4) A method to match the parameterized octagonal template with the segmentation image and extract the octagon midline from the template as the navigation line is proposed.

(5) Experimental results show that the navigation line detection method proposed in this paper can stably and reliably detect navigation lines for the *L.barbarum* Garden, laying the foundation for precise navigation of a self-moving platform in complex and unstructured *L.barbarum* Garden environments.

To realize visual navigation of the self-moving platforms under *L.barbarum* Garden environments, there is still some work to be done: 1) Carry out the navigation experiment under *L.barbarum* Garden environments based on the edge detection and navigation line detection methods above. 2) There are agronomy links of *L.barbarum* in early winter and early spring. During these periods, there is no obvious colour difference between the plant column region and the soil region, and it is a difficult problem to realize edge detection.

ACKNOWLEDGMENTS

The authors thank Ningxia University for providing hardware support. The authors also thank Xiaoqiang Ren for technical support and image processing hardware support.

REFERENCES

Ball, D., Upcroft, B., Wyeth, G., et al., "Vision-based Obstacle Detection and Navigation for an Agricultural Robot,Journal of Field Robotics, Vol.33, No.8, pp.1107–1130 (2016).

Ding, W., Li, Y., Liu, H., "Efficient vanishing point detection method in unstructured road environments based on dark channel prior," IET Computer Vision, Vol.10, No.8, pp. 852–860 (2016).

Ebrahimpou，R., Rasoolinezhad，R., Hajiabolhasani, Z., et al., "Vanishing point detection in corridors: using Hough transform and K-means clustering," IET Computer Vision, Vol.6, No.1, pp.40－51 (2012).

Erhan, C., Sariyanidi, E., Sencan, O., et al., "Patterns of approximated localized moments for visual loop closure detection," IET Computer Vision, Vol.11, No.3, pp.237–245 (2017).

Gou, B., Cheng, Y., "Automatic centroid extraction method for noisy star image," IET IMAGE PROCESSING, Vol.12, No.6, pp.856–862

(2018).
Jiang, D., Wang, S., Zeng, Y., et al., "Agricultural robot visual de-hazing method based on image segmentation map," Nongye Jixie Xuebao/Transactions of the Chinese Society for Agricultural Machinery, Vol.47, No.11, pp.25–31 (2016).
Li, J., Chen, B., Liu, Y., et al., "Study on Image Detection Method of Navigation Route for Cotton Harvester," Proc. International Conference on Computer-Aided Design, Manufacturing, Modeling and Simulation, Chongqing, China, January (2012).
Liu, J., Jayakumar, P., Stein, J. L., et al., "A nonlinear model predictive control formulation for obstacle avoidance in high-speed autonomous ground vehicles in unstructured environments," VEHICLE SYST DYN, Vol.56, No.6, pp.853–882 (2018).
Mannar, S., Thummalapeta, M., Saksena, S. K., et al., "Vision-based Control for Aerial Obstacle Avoidance in Forest Environments," IFAC PAPERSONLINE, Vol.51, No.1, pp.480–485 (2018).
Meng, Q., Hao, X., Zhang, Y., et al., "Guidance Line Identification for Agricultural Mobile Robot Based on Machine Vision," Proc. 2018 IEEE 3rd Advanced Information Technology, Electronic and Automation Control Conference (IAEAC), Chongqing, China, October, pp.1887–1893 (2018).
Miao, Z., M, C., Gao, Z., et al., "Hidden feature extraction for unstructured agricultural environment based on supervised kernel locally linear embedding modeling," ADVANCES IN MANUFACTURING, Vol.6, No.4, pp.409–418 (2018).
Roviramás, F., Reid, J.F., Zhang, Q., "Automated agricultural equipment navigation using stereo disparity images," Trans Am Soc Agric Eng, Vol.47, No.4, pp.1289–1300 (2004).
Tang, X. and Ji, Y., "Research on agricultural intelligent robot based on path planning," Advances in Intelligent Systems and Computing, Vol. 613, pp.108–115 (2018).
Winterhalter, W., Fleckenstein, F.V., Dornhege, C., et al., "Crop Row Detection on Tiny Plants With the Pattern Hough Transform," IEEE Robotics and Automation Letters, Vol.3, No.4, pp.3394–3401 (2018).
Yang, T., Li, P., Zhang, H., et al., "Monocular Vision SLAM-Based UAV Autonomous Landing in Emergencies and Unknown Environments," ELECTRONICS, Vol.7, No.735, (2018).
Yang, S., Mei, S., Zhang, Y., "Detection of Maize Navigation Centerline Based on Machine Vision," Proc. 6th International-Federation-of-Automatic-Control (IFAC) Conference on Bio-Robotics (BIOROBOTICS), Beijing, China, July 2018, pp. 570–575 (2018).
Yohannan, B. and Chandy, D. A., "A novel approach for fusing LIDAR and visual camera images in unstructured environment," Proc. International Conference on Advanced Computing and Communication, Coimbatore, INDIA, January 2017 (2017).
Zhai, Z.Q., Zhu, Z.X., Du, Y.F., et al., "Multi-crop-row detection algorithm based on binocular vision," Biosyst Eng, Vol.150, pp. 89–103 (2016).
Zhang, S., Wang, Y., Zhu, Z., et al., "A tractor path tracking control system based on binocular vision and pure pursuit model is designed," Information Processing in Agriculture, Vol.5, No.4, pp.422–432 (2018).
Zhao, T., Noguchi, N., Yang, L., et al., "Fast edge detection method for wheat field based on visual recognition," Nongye Jixie Xuebao/Transactions of the Chinese Society for Agricultural Machinery, Vol.47, No.11, pp. 32–37 (2016).
Zhou, J., Chen, Q. and Liang, Q., "Vision navigation of agricultural mobile robot based on reinforcement learning," Nongye Jixie Xuebao/Transactions of the Chinese Society for Agricultural Machinery, Vol.45, No.2, pp. 53–58 (2014).

基於遺傳演算法的枸杞園導航線檢測方法研究

李茂強　　劉志峰
合肥工業大學機械工程學院

摘 要

"通用自主移動承載平臺+作業模組"模式是實現枸杞智慧化生產的必由之路，株列與土壤區域分割及導航線檢測問題是自主移動平臺自主導航的難點。針對株列與土壤區域分割問題，採用了一種基於神經網路和 Otsu 的分割方法，實驗表明基於該方法能有效進行圖像分割；提出了一種雜訊去除方法，該方法能有效去除株列區域的雜訊和土壤區域的雜訊；針對已完成分割的圖像的導航線檢測問題，構建參數化八邊形範本，以參數化八邊形範本圖像與分割圖像匹配，以匹配重疊度為適應度函數，基於遺傳演算法優化八邊形範本參數，以優化後的八邊形範本提取中線作為導航線，實驗表明該方法能有效檢測導航線，為枸杞園複雜非結構化環境下自主移動平臺精准導航奠定了基礎。